2017 IEEE/RSJ International Conference on Intelligent Robots and Systems (IROS)
September 24–28, 2017, Vancouver, BC, Canada

Robust Initialization of Monocular Visual-Inertial Estimation on Aerial Robots

Tong Qin and Shaojie Shen

***Abstract*— In this paper, we propose a robust on-the-fly estimator initialization algorithm to provide high-quality initial states for monocular visual-inertial systems (VINS). Due to the non-linearity of VINS, a poor initialization can severely impact the performance of either filtering-based or graph-based methods. Our approach starts with a vision-only structure from motion (SfM) to build the up-to-scale structure of camera poses and feature positions. By loosely aligning this structure with pre-integrated IMU measurements, our approach recovers the metric scale, velocity, gravity vector, and gyroscope bias, which are treated as initial values to bootstrap the nonlinear tightly-coupled optimization framework. We highlight that our approach can perform on-the-fly initialization in various scenarios without using any prior information about system states and movement. The performance of the proposed approach is verified through the public UAV dataset and real-time onboard experiment. We make our implementation open source, which is the initialization part integrated in the VINS-Mono[1].**

I. Introduction

Visual-inertial fusion is currently a hot topic in robotics communities. The accurate state estimation is required in a wide range of applications, such as aerial graphics, autonomous driving, transportation, surveillance and rescue. Traditional vision-only algorithms, such as [1]–[5], can estimate pose and construct the structure of environments. However, since the scale can not be recovered from a single camera, these algorithms can not be directly used in real-world application, especially for autonomous navigation. Usually, the inertial measurement unit (IMU) is treated as complementary sensor for vision based algorithms [6]–[12]. By fusing the metric measurement from IMU, the scale, as well as roll and pitch angle can be fully recovered. In addition, the IMU measurement can assist vision when tracking lost due to illumination change, texture-less area and motion blur caused by aggressive motion. The performance is dramatically improved with the help of IMU. One camera and a low-cost IMU constitute the minimum sensor set to provide sufficient self and environment awareness, which can be easily got on any smart platform.

Due to the nonlinearity of visual-inertial systems, the performance of monocular estimators [6, 8, 12]–[15] heavily rely on the accuracy of initial values (gravity, velocity, bias, and depth of features). A poor initialization will decrease convergence speed or even lead to totally incorrect estimates.

All authors are with the Department of Electronic and Computer Engineering, Hong Kong University of Science and Technology, Hong Kong, China. tong.qin@connect.ust.hk, eeshaojie@ust.hk
This work was supported by the Hong Kong Research Grants Council, Early Career Scheme, project no. 26201616.

[1]https://github.com/HKUST-Aerial-Robotics/VINS-Mono

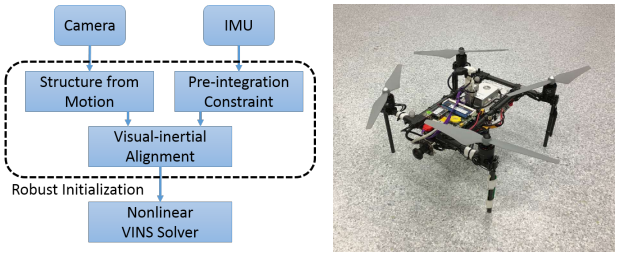

(a) (b)

Fig. 1. (a) The main structure of our initialization procedure. (b) The self-developed quadrotor with one forward-looking camera which is used in the indoor closed-loop experiment.

Especially for aerial robots which have full six degrees of freedom, accurate initial values are crucial. However, it is hard to obtain accurate initial states for the monocular visual-inertial system. On one hand, the metric scale cannot be obtained from monocular camera. On the other hand, non-zero acceleration motion is required to initialize the metric scale. This leads to unknown initial attitude (gravity vector) and velocity. In particular, during time-limited search and rescue missions, careful initialization with the MAV sitting stationary or moving along certain pattern is often infeasible. It is desirable to launch the MAV quickly and initialize the estimator without any prior knowledge about dynamical motion. In addition, vision algorithm is fragile during fast motion or under strong illumination change. The estimator will easily fail when the visual tracking is lost. This suggests that the development of on-flight automatically re-initialization is necessary. All these issues drive us to find a robust system which is capable of on-the-fly initialization to recover all critical states.

In this paper, we propose an approach which allows a monocular visual-inertial system to be initialized on-the-fly. Initial velocity, gravity vector, scale as well as gyroscope bias are calibrated in the initialization procedure. We first perform vision-only structure from motion (SfM), then loosely align IMU measurements with SfM results to get metric initial states. The performance of our approach is proved by public dataset and real-time onboard experiments in indoor and outdoor environments.

We highlight that our contribution in threefold:

- A robust visual-inertial initialization procedure, which can provide initial states for on-the-fly aerial robots.
- At the system level, we applied the proposed approach into sliding-window based monocular visual-inertial system. Onboard closed-loop autonomous flight

experiments are performed.
- Open source code for the community.

The rest of the paper is structured as follows. In Sect. II, we discuss the relevant literature. The motivation and system overview are discussed in Sect. III. In Sect. IV, we present the methodology. Implementation details and experimental evaluations are presented in Sect. V. Finally, the paper is finished with the conclusion in Sect. VI.

II. Related Work

There are a large number of studies on visual-inertial state estimation problem. Traditional solutions with either monocular or stereo cameras are classified into two categories, filtering-based frameworks [13, 15]–[18] and graph-based optimization frameworks [6, 8, 12, 14]. Filtering-based approaches have an advantage in faster processing since it continuously marginalizes past states. However, linearizing states early may lead to sub-optimal results. Graph-based approaches benefit from the capacity of iterative re-linearization but they usually suffer from the computational requirement. In general, some of initial states (velocity, gravity orientation, and IMU bias) are assumed to be known or neglected, or the system should stay stationary and horizontal before launch. Without prior information, most methods are not suitable for dynamically taking off or on-the-fly initialization.

Our earlier works [7, 12] proposed a linear estimator initialization method by leveraging known relative rotations from short-term gyroscope integration. This method performs well in indoor environments. However, it fails in environments where feature depths are distributed throughout a wide range (e.g. outdoor environments) due to the incapability of modeling the sensor noise in the raw projective formulation. Also, our earlier work didn't take bias into consideration. Recently, a closed-form solution has been introduced in [19]. Later, a revision of this closed-form solution is proposed in [20]. Authors added gyroscope bias calibration in this method. However, the original formulation was changed into a nonlinear and nonconvex form. In both works, authors fail to model the accuracy of inertial integration at different time durations. It is known that the accuracy of inertial integrated accuracy drops significantly as the time duration increases. In [9], a re-initialization and failure recovery algorithm based on SVO [2] is proposed. It is a practical method in the loosely-coupled visual-inertial system. Inertial measurements are used first to stabilize the MAV's attitude, then the SVO is launched for position feedback. This work assumed that the drone should be held nearly horizontally at the beginning. Also, another distance sensor, TeraRanger, is used for height measurement. [21] proposed another initialization algorithm for loosely-coupled filtering system, which used optical flow between two consecutive frames to extract velocity and dominant terrain plane. This method also required no or little motion in initialization step since the initial attitude should be aligned with gravity.

Vision-only structure from motion (SfM) techniques are able to recover the relative rotation and translation up to an unknown scale factor within multiple cameras poses [22]. Such methods are currently used in state-of-the-art visual navigation for MAVs [2, 9]. However, the unavailability of metric scale and absolute attitude can result in instability in autonomous flight. [23] proposed a method to compute the gravity vector and scale factor, and provided initial metric values for the state estimation filter. This method was based on analyzing the relationship between SfM and inertial integration. [24] presents an IMU initialization algorithm which based on the monocular ORB-SLAM [4] recently. An initial estimation of the scale, gravity direction, velocity and IMU biases are computed for the visual-inertial full BA given a set of keyframes processed by a monocular SLAM. However, it was reported that the time required for scale convergence can be longer than 10 seconds, which is inappropriate for robotic navigation tasks that require scale estimation at the beginning. Our framework is similar with [24]. We ignore acceleration bias in the initial step to ensure fast initialization. We find out that acceleration bias coupled with gravity usually lacks observability. Details about acceleration bias calibration are discussed in Sect. IV-E.

For IMU measurement processing, heavy and repeated propagation is usually needed when the starting states changed. Recently, one efficient technique to deal with it is called pre-integration, which avoids repeating integrating IMU measurement. This algorithm was first proposed in [25], which reparametrized IMU measurements into relative motion constraints. [8] considered on-manifold uncertainty of this technique. However, IMU bias was ignored in his formulation. Furthermore, [26] improved preintegration theory, which considered on-manifold uncertainty as well as modeled posterior bias correction.

III. Overview

Visual and inertial measurements are two complementary resources. The vision represents up-to-scale global structure, and IMU introduces metric incremental information. Absolute scale and velocity are not available in monocular camera. To initialize the metric scale, non-zero accelerated motion is required, which leads to unknown initial attitude (gravity vector) and velocity at the beginning. So we cannot assume estimators start in the stationary state. What's worse, the IMU is usually influenced by non-ignorable bias. It is hard to directly fuse these two factors together without a good initial guess. A bad initial value will lead the estimator diverging or falling into a local minimum. To improve the success rate of the monocular visual-inertial system, a robust initialization procedure is required.

Monocular vision-only SLAM or structure from motion (SfM) is easier to be initialized than visual-inertial system. Vision-only system can easily bootstrap itself by Eight-point [22], Five-point [27], homogeneous and fundamental method. Then Bundle Adjustment [28] is followed to refine the structure. Given an up-to-scale visual structure, we can align IMU measurements into this structure to extract initial values (gravity, velocity and bias) of visual-inertial

system. Inspired by this, we adopt a loosely coupled visual-inertial initialization procedure. We construct the visual-only structure firstly, then align this structure with IMU pre-integrations to recover initial values. The pipeline of our proposed method is shown in Fig. 1(a).

IV. Methodology

We start with defining notations. We consider $(\cdot)^w$ as world frame, where gravity vector is along with z axis. $(\cdot)^v$ is the reference frame in SfM, which is an arbitrarily fixed frame in visual structure, irrelevant to inertial measurement. $(\cdot)^w_b$ is body frame with respect to world frame. We treat the IMU frame as the body frame, which means IMU frame is aligned with body frame. b_k is the body frame while taking the k^{th} image. $(\cdot)^v_c$ is camera frame with respect to the visual reference frame. c_k is the camera frame while taking the k^{th} image. We use $\hat{(\cdot)}$ to denote sensor measurements, which may be affected by noise and bias. We use $\bar{(\cdot)}$ to denote up-to-scale parameters in SfM structure. We use quaternion $\mathbf{q}$ to denote rotation. $\otimes$ is the two quaternion multiplication operation. $\mathbf{g}^w = [0, 0, g]^T$ is the gravity vector in the world frame. $\mathbf{g}^v$ is the gravity vector in the visual reference frame.

We assume that the intrinsic calibration of the camera and extrinsic calibration between the camera and IMU is known in the initialization step. In fact, we do not need a very precise extrinsic calibration since we will continuously refine it in the nonlinear optimization (Sect. IV-D).

A. Vision-Only Structure

The initialization procedure starts with a vision-only structure, which estimates a graph of up-to-scale camera poses and feature positions. Our method is based on the sliding-window based method [8, 12], which maintains several spacial-separate image frames. Spacial frames are selected by enough parallax near the neighbor. Sparse features are extracted [29] and tracked [30] among these frames. The feature correspondences are used to construct the visual structure inside the window.

As a common technique used in computer vision, we first choose two frames which contain sufficient feature parallax. Then Five-point method [27] is used to recover the relative rotation and up-to-scale translation between these two frames. Then we arbitrarily set the scale and triangulate all features observed in these two frames. Based on these triangulated features, Perspective-n-Point (PnP) method is performed to estimate poses of other frames in the window. Finally, a global full Bundle Adjustment [28] is applied to minimize the total re-projection error of all feature observations. After that, we get all frame poses ($\bar{\mathbf{p}}^v_{c_k}$,$\mathbf{q}^v_{c_k}$) and feature positions. Assume that we have the prior of the extrinsic parameter $(\mathbf{p}^c_b, \mathbf{q}^c_b)$ between camera frame and IMU (body) frame, all variables can be translated from camera frame to the IMU frame,

$$\begin{aligned} \mathbf{q}^v_{b_k} &= \mathbf{q}^v_{c_k} \otimes \mathbf{q}^c_b \\ s\bar{\mathbf{p}}^v_{b_k} &= s\bar{\mathbf{p}}^v_{c_k} + \mathbf{q}^v_{c_k}\mathbf{p}^c_b \end{aligned} \tag{1}$$

s is unknown scale, which will be solved in the next.

B. IMU Pre-Integration

IMU measurements run at a higher frequency than visual measurements. Usually, dozens of IMU measurements exist between two consecutive visual frames. We pre-integrate [26] these IMU measurements in the local frame, and treat this integration result as the incremental metric constraint.

We denote IMU measurements (angular velocity and acceleration) as $\hat{\boldsymbol{\omega}}^b$, $\hat{\mathbf{a}}^b$. These measurements are affected by bias $\mathbf{b}$ and noise $\boldsymbol{\eta}$,

$$\begin{aligned} \hat{\boldsymbol{\omega}}^b(t) &= \boldsymbol{\omega}^b(t) + \mathbf{b}_g + \boldsymbol{\eta}_g \\ \hat{\mathbf{a}}^b(t) &= \mathbf{q}^w_b(t)^{\mathrm{T}}(\mathbf{a}^w(t) + \mathbf{g}^w) + \mathbf{b}_a + \boldsymbol{\eta}_a. \end{aligned} \tag{2}$$

Given two time instants that correspond to images frame b_k and b_{k+1}, we can pre-integrate linear acceleration and angular velocity in the local frame b_k:

$$\begin{aligned} \boldsymbol{\alpha}^{b_k}_{b_{k+1}} &= \iint_{t\in[k,k+1]} \boldsymbol{\gamma}^{b_k}_{b_t}\hat{\mathbf{a}}(t)dt^2 \\ \boldsymbol{\beta}^{b_k}_{b_{k+1}} &= \int_{t\in[k,k+1]} \boldsymbol{\gamma}^{b_k}_{b_t}\hat{\mathbf{a}}(t)dt \\ \boldsymbol{\gamma}^{b_k}_{b_{k+1}} &= \int_{t\in[k,k+1]} \boldsymbol{\gamma}^{b_k}_{b_t} \otimes \begin{bmatrix} 1 \\ \frac{1}{2}\hat{\boldsymbol{\omega}}(t) \end{bmatrix} dt, \end{aligned} \tag{3}$$

$\boldsymbol{\alpha}^{b_k}_{b_{k+1}}, \boldsymbol{\beta}^{b_k}_{b_{k+1}}, \boldsymbol{\gamma}^{b_k}_{b_{k+1}}$ represent relative position, velocity, and rotation constraints respectively. It can be seen that inertial measurements are typically integrated to form relative motion constraints which is independent of initial position and velocity of frame b_k.

C. Visual-Inertial Alignment

We get the up-to-scale camera poses from SfM (Sect. IV-A), and metric measurements from IMU pre-integration (Sect. IV-B). In this section, we detail our approach to align these two parts.

1) Gyroscope Bias Calibration: Considering two consecutive frames b_k and b_{k+1} in the window, we have the relative rotation $\mathbf{q}^v_{b_k}$ and $\mathbf{q}^v_{b_{k+1}}$ from the visual structure, as well as relative constraint $\hat{\boldsymbol{\gamma}}^{b_k}_{b_{k+1}}$ from the IMU pre-integration. We estimate the gyroscope bias by minimizing the error between these two terms:

$$\begin{aligned} &\min_{\delta b_g} \sum_{k\in\mathcal{B}} \left\| {\mathbf{q}^v_{b_{k+1}}}^{-1} \otimes \mathbf{q}^v_{b_k} \otimes \boldsymbol{\gamma}^{b_k}_{b_{k+1}} \right\|^2 \\ &\boldsymbol{\gamma}^{b_k}_{b_{k+1}} \approx \hat{\boldsymbol{\gamma}}^{b_k}_{b_{k+1}} \otimes \begin{bmatrix} 1 \\ \frac{1}{2}\frac{\partial \boldsymbol{\gamma}^{b_k}_{b_{k+1}}}{\partial \mathbf{b}_g}\delta\mathbf{b}_g \end{bmatrix}, \end{aligned} \tag{4}$$

where $\mathcal{B}$ indexes all frames in the window. In the second equation, we linearize the rotation constraint with respect to gyroscope bias. Aligning rotation in visual structure with relative constraint $\boldsymbol{\gamma}$, we can get the estimation of $\mathbf{b}_g$. Then we update $\hat{\boldsymbol{\alpha}}^{b_k}_{b_{k+1}}, \hat{\boldsymbol{\beta}}^{b_k}_{b_{k+1}}$ with respect to $\mathbf{b}_g$.

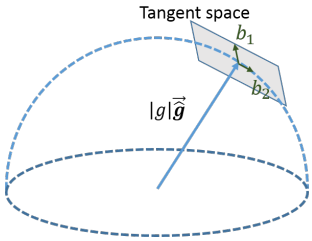

Fig. 2. Since the magnitude of gravity is known, the degrees-of-freedom of the gravity is two. $\mathbf{g}$ lies on a sphere where the radius is the known magnitude $|g|$. We parameterize the gravity around current estimate as $g \cdot \bar{\hat{\mathbf{g}}} + w_1\mathbf{b}_1 + w_2\mathbf{b}_2$, where $\mathbf{b}_1$ and $\mathbf{b}_2$ are two orthogonal basis spanning the tangent space.

2) Initializing Velocity, Gravity Vector and Metric Scale: We define variables that are estimated in this step as

$$\mathcal{X}_I = \left[\mathbf{v}^v_{b_0},\, \mathbf{v}^v_{b_1},\, \cdots \mathbf{v}^v_{b_n},\, \mathbf{g}^v,\, s\right], \tag{5}$$

where s is the scale parameter that aligns the visual structure to the actual metric scale implicitly provided by IMU measurements. The following equation describes the relationship between metric position and velocity constraint with visual structure,

$$\begin{aligned}\hat{\mathbf{z}}^{b_k}_{b_{k+1}} &= \begin{bmatrix}\hat{\boldsymbol{\alpha}}^{b_k}_{b_{k+1}} \\ \hat{\boldsymbol{\beta}}^{b_k}_{b_{k+1}}\end{bmatrix} = \mathbf{H}^{b_k}_{b_{k+1}}\mathcal{X}_I + \mathbf{n}^{b_k}_{b_{k+1}} \\ &\approx \begin{bmatrix}-\mathbf{q}^{b_k}_v\Delta t_k & \mathbf{0} & \frac{1}{2}\mathbf{q}^{b_k}_v\Delta t_k^2 & \mathbf{q}^{b_k}_v(\bar{\mathbf{p}}^v_{b_{k+1}} - \bar{\mathbf{p}}^v_{b_k}) \\ -\mathbf{q}^{b_k}_v & \mathbf{q}^{b_k}_v & \mathbf{q}^{b_k}_v\Delta t_k & \mathbf{0}\end{bmatrix}\begin{bmatrix}\mathbf{v}^v_{b_k} \\ \mathbf{v}^v_{b_{k+1}} \\ \mathbf{g}^v \\ s\end{bmatrix}\end{aligned} \tag{6}$$

In the above formula, $\mathbf{q}^v_{b_k}, \bar{\mathbf{p}}^v_{b_k}, \bar{\mathbf{p}}^v_{b_{k+1}}$ are obtained from the visual structure. $\mathbf{q}^{b_k}_v$ is the inverse rotation of $\mathbf{q}^v_{b_k}$. Δt_k is the time interval between two consecutive frames. By solving the this least square problem:

$$\min_{\mathcal{X}_I}\sum_{k\in\mathcal{B}}\left\|\hat{\mathbf{z}}^{b_k}_{b_{k+1}} - \mathbf{H}^{b_k}_{b_{k+1}}\mathcal{X}_I\right\|^2, \tag{7}$$

we can get velocities and the gravity vector in the visual reference frame $(\cdot)^v$, as well as the scale parameter. Translational components $\bar{\mathbf{p}}^v$ from the visual structure will be scaled to metric units. The estimated gravity will undergo another round of refinement by enforcing the norm constraint.

3) Gravity Refinement: The gravity vector obtained from the previous step can be refined by constraining the magnitude of the gravity vector. In most cases, the magnitude of the gravity vector is known. However, if we directly add this norm constraint into the optimization problem in (7), it will become nonlinear and hard to solve. Here, we use a method to enforce the gravity norm by optimizing the 2D error state on its tangent space. Since the magnitude of gravity is known, the degree of freedom of the gravity is two and we can parameterize the gravity with two variables on its tangent space. We parameterize the gravity as $g \cdot \bar{\hat{\mathbf{g}}} + w_1\mathbf{b}_1 + w_2\mathbf{b}_2$, where g is the magnitude of gravity, $\bar{\hat{\mathbf{g}}}$ is the direction vector of current estimation, $\mathbf{b}_1$ and $\mathbf{b}_2$ are two orthogonal basis spanning the tangent plane. w_1 and w_2 are corresponding displacements towards $\mathbf{b}_1$ and $\mathbf{b}_2$, respectively. We can use Gram-Schmidt process to find one set of $\mathbf{b}_1, \mathbf{b}_2$ easily. In this way, we reparameterize gravity by two states on its tangent space, as shown in Fig. 2. Then we substitute $\mathbf{g}$ in (6) by $g\cdot\bar{\hat{\mathbf{g}}} + w_1\mathbf{b}_1 + w_2\mathbf{b}_2$ and it is also in linear form. This process iterates several times until $\hat{\mathbf{g}}$ converges.

After refining gravity vector, we rotate all variables from visual reference frame $(\cdot)^v$ to the world frame $(\cdot)^w$ according to the gravity vector. At this point, the initialization procedure is completed and these metric values will be fed for a tightly-coupled nonlinear visual-inertial estimator.

D. Nonlinear VINS Estimator

After obtaining all essential initial values, we can launch our tightly-coupled VINS estimator [8, 31]. Here, we briefly describe our graph optimization-based solution to the nonlinear visual-inertial system.

The definition of full states in a sliding window with N IMU frames and M features are (the transpose is ignored):

$$\begin{aligned}\mathcal{X} &= \left[\mathbf{x}_0,\, \mathbf{x}_1,\, \cdots \mathbf{x}_n,\, \mathbf{x}^b_c,\, \lambda_0,\, \lambda_1,\, \cdots \lambda_m\right] \\ \mathbf{x}_k &= \left[\mathbf{p}^w_{b_k},\, \mathbf{v}^w_{b_k},\, \mathbf{q}^w_{b_k},\, \mathbf{b}_a,\, \mathbf{b}_g\right], k \in [0, n] \\ \mathbf{x}^b_c &= \left[\mathbf{p}^b_c,\, \mathbf{q}^b_c\right],\end{aligned} \tag{8}$$

where the k-th IMU state consists of the position $\mathbf{p}^w_{b_k}$, velocity $\mathbf{v}^w_{b_k}$, orientation $\mathbf{q}^w_{b_k}$ of body frame b_k with respect to world frame w, and IMU bias $\mathbf{b}_a$, $\mathbf{b}_g$. 3D features are parameterized by their inverse depth λ when first observed in camera frame, and $\mathbf{x}^b_c$ is the extrinsic transformation from camera frame c to body frame b. The estimation is formulated as a nonlinear least-square problem,

$$\begin{aligned}\min_{\mathcal{X}}\Bigg\{&\left\|\mathbf{r}_p - \mathbf{H}_p\mathcal{X}\right\|^2 + \sum_{k\in\mathcal{B}}\left\|\mathbf{r}_{\mathcal{B}}(\hat{\mathbf{z}}^{b_k}_{b_{k+1}},\, \mathcal{X})\right\|^2_{\mathbf{P}^{b_k}_{b_{k+1}}} + \\ &\sum_{(l,j)\in\mathcal{C}}\rho(\left\|\mathbf{r}_{\mathcal{C}}(\hat{\mathbf{z}}^{c_j}_l,\, \mathcal{X})\right\|^2_{\mathbf{P}^{c_j}_l})\Bigg\},\end{aligned} \tag{9}$$

where $r_{\mathcal{B}}(\hat{\mathbf{z}}^{b_k}_{bk+1}, \mathcal{X})$ and $r_{\mathcal{C}}(\hat{\mathbf{z}}^{c_j}_l, \mathcal{X})$ are nonlinear residual functions for inertial and visual measurements. $||\cdot||$ is the Mahalanobis distance weighted by covariance $\mathbf{P}$. To be specific, $r_{\mathcal{B}}$ is the residual of IMU factor which connects pair of consecutive frames b_k and b_{k+1} by the integration of inertial measurements $\hat{\mathbf{z}}^{b_k}_{b_{k+1}}$. $r_{\mathcal{C}}$ is the residual of vision factor which builds the connection between landmark measurements $\hat{\mathbf{z}}^{c_j}_l$ and states through re-projection function. $\rho(\cdot)$ is the robust huber norm [32]. Past states are marginalized and converted to the prior information, $\{\mathbf{r}_p,\, \mathbf{H}_p\}$. The detailed optimization can be found at [33].

E. Discussions

To achieve full observability of the monocular VINS except for the global position shift and the yaw angle, sufficient excitation in both vision and IMU factor is required. The observability of the vision module can be ensured by selecting a number of spacial-separated frames which contain sufficient

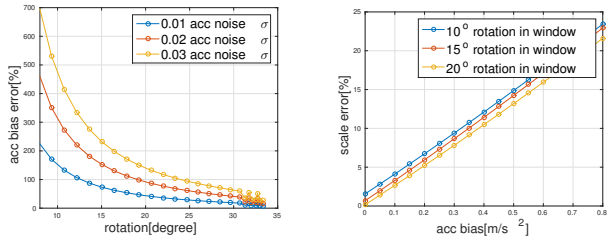

(a) (b)

Fig. 3. (a) The x-axis represents the average rotation change in the initialization step. The y-axis represents the estimation error of acceleration bias under different measurement noise. It can be seen that it is difficult to distinguish acceleration bias unless sufficient rotation in movement. (b) The x-axis represents different acceleration bias. The y-axis represents the estimated scale error of proposed algorithm without consideration of acceleration bias. It can be seen that limited acceleration bias will not severely destroy the algorithm. The margin of bearable acceleration bias is up to 0.3 m/s^{-2} in this simulation if we can accept 10% visual scale error in initial guess.

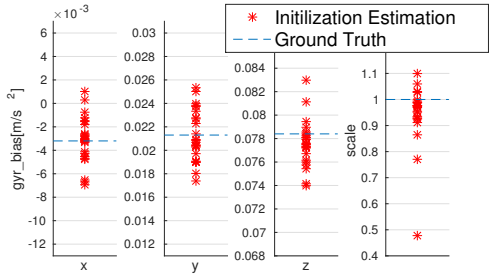

Fig. 4. Gyroscope bias and scale recovered in the initialization procedure in MH_01_easy dataset. The figure contains the results in 25 tests with different start time.

parallax. However, the IMU measurements within the SfM window may not render the whole system observable. For a rotorcraft MAV, degenerate motions such as rectilinear trajectories or zero-acceleration motions are unavoidable. This is a common issue when trying to use monocular VINS on aerial robots. Intuitively, we can reject small acceleration motion by checking the variation of $\hat{\boldsymbol{\alpha}}_{b_{k+1}}^{b_k}$, $\hat{\boldsymbol{\beta}}_{b_{k+1}}^{b_k}$ in the initialization step. The initialization procedure only starts when sufficient excitation is included in the windowed IMU measurements.

Acceleration bias is difficult to calibrate in initialization procedure, since acceleration is usually coupled with gravity under small rotation. To figure out the observability of acceleration bias along with movement, we design the following simulated experiment. In the simulation environment, the aerial robot does accelerated movement with different levels of rotation. The acceleration bias is constant [0.1,0.1,0.1]$m \cdot s^{-2}$ with noise whose standard deviation is from 0.01 to 0.03$m \cdot s^{-2}$. 15 spatially separated frames are kept in the window. Image noise is not included, which means an accurate visual structure. Also, gyroscope bias and noise are not included, which can eliminate the influence of gyroscope. To calibrate the acceleration bias in proposed framework, we can linearize position and velocity constraints $\hat{\boldsymbol{\alpha}}_{b_{k+1}}^{b_k}, \hat{\boldsymbol{\beta}}_{b_{k+1}}^{b_k}$ with respect to acceleration bias, as the same step in eq. 4. Then take the acceleration bias into eq. 6. The calibration results of acceleration bias are shown in Fig. 3(a). The x-axis is the average rotation change along three axes in the window, and the y-axis is the magnitude of error of calibrated bias. From the figure, we can see that at least 30-degree rotation is needed if we want to fully calibrated acceleration bias in short initialization procedure. In the real scenario, such aggressive rotation movement in the beginning is infeasible due to the dynamical constraints of the robotic platform.

In another simulation, we test the performance of visual-inertial alignment when the acceleration bias is neglected. In this simulation, we take image noise (0.5 pixel in σ), gyroscope bias ([0.003,0.02,0.08]$rad \cdot s^{-1}$) and gyroscope noise (0.0024$rad \cdot s^{-1}$in σ) into consideration. The error of scale along with acceleration bias is shown in Fig. 3(b). The x-axis is the magnitude of acceleration bias, and the y-axis is the percentage error of scale. The influence caused by acceleration is linear in this scope. The tolerance of acceleration bias is up to $0.3m \cdot s^{-2}$ if we can accept 10% percent scale error. $0.3m \cdot s^{-2}$ bias is an extreme value for normal IMU in usual. Ignoring acceleration bias does not dramatically influence initialization result.

From the simulation, we can see that it is hard to distinguish acceleration bias from gravity unless sufficiently excited rotation is executed. This is hard to achieve in practice due to the dynamical constraints of the robotic platform. Neglecting acceleration bias will not pose significant negative impact on the initialization result. To this end, we leave the estimation of the acceleration bias estimation to the nonlinear optimization (Sect. IV-D).

V. Experimental Results

We first validate our algorithm with the publicly available MAV Visual-Inertial Datasets in the ASL Dataset [34]. Then we apply our method to real-world indoor and outdoor environments.

A. Performance on Public Datasets

The MAV Visual-Inertial Datasets in ASL Dataset are collected onboard a micro aerial vehicle. The dataset contains stereo images (Aptina MT9V034 global shutter, WVGA monochrome, 20 FPS), synchronized IMU measurements (ADIS16448, angular rate, and acceleration, 200 Hz), and ground truth states (VICON and Leica MS50). We only use one camera from stereo images set.

1) Initial Values Recovery: We use the MH_01_easy dataset for evaluation. In this dataset, the gyroscope bias and accelerometer bias are around [-0.0032, 0.021, 0.078]$rad \cdot s^{-1}$ and [-0.0032, 0.026, 0.076]$m \cdot s^{-2}$ in x, y and z axes respectively. In our algorithm, we maintain at least 15 frames for initial visual structure. We estimate gyroscope bias in the initialization phase, while leave the accelerometer bias estimation to the following nonlinear optimization. To verify the capability of on-the-fly initialization, we randomly select start times in the dataset, which means our algorithm starts

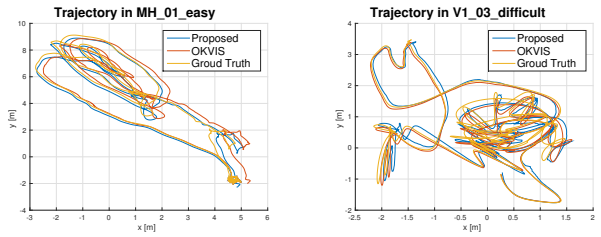

(a) (b)

Fig. 5. Trajectory in MH_01_easy and V1_01_difficult respectively. Our proposed method is compared with state-of-art stereo visual-initial algorithm, OKVIS.

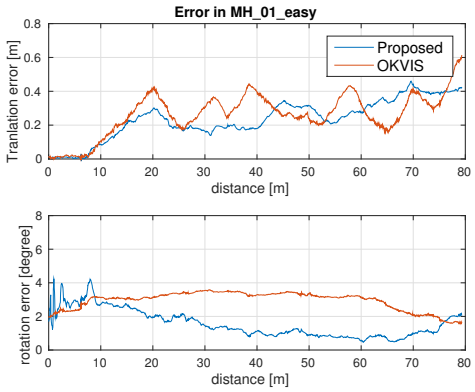

Fig. 6. Translation and rotation error in MH_01_easy.

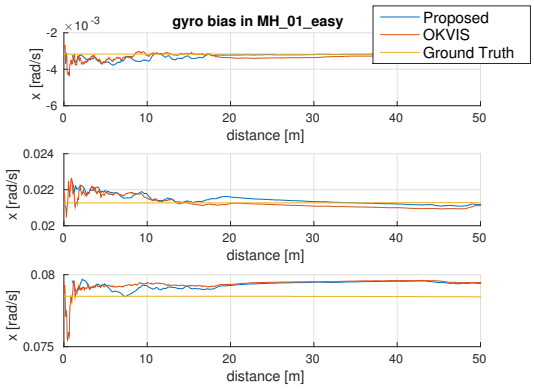

Fig. 7. Gyroscope bias in MH_01_easy.

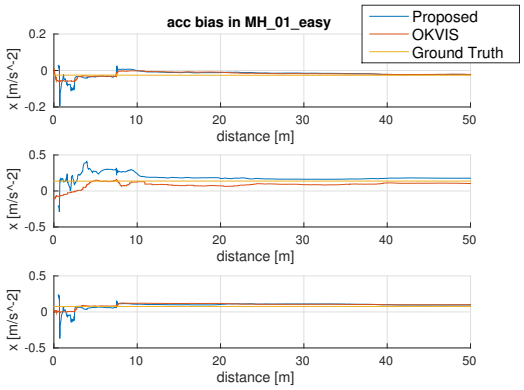

Fig. 8. Acceleration bias in MH_01_easy.

without any prior information when the drone is flying. Fig. 4 shows the gyroscope bias and scale calibration performance in 25 tests with the different start times in MH_01_easy dataset. The four sub-figures are gyroscope bias in xyz axis and scale respectively. The average error of gyroscope bias in two dominant direction x and y are [8.59,1.82]% respectively. And the average scale error is 8.09%. If we define the scale error less than 10% is successful initialization, our procedure performs 84% success rate in this dataset. In fact, the nonlinear estimator can be successfully bootstrapped even the initial scale error is over 30%.

2) Overall Performance: We choose two datasets, MH_01_easy, V1_03_difficult to show the whole performance of our visual-inertial odometry. In these experiments, we compare proposed method with OKVIS [6], which is the state-of-art visual-inertial algorithm working with stereo cameras. The whole trajectories are shown in Fig. 5. Our monocular system can achieve the same accuracy as the stereo system.

The error plot of MH_01_easy is shown in Fig. 6. The x-axis is distance, while the y-axis represents translation error and rotation error respectively. Proposed algorithm achieve nearly the same accurate result as the stereo system in translation. The gyroscope bias estimation is shown in Fig. 7. In the beginning, proposed method presents a stable gyroscope bias estimation because of a good initial guess from initialization procedure. Fig. 8 shows the acceleration bias estimation. Although we neglect the acceleration bias in the initialization procedure, the bias estimation converges gradually along with the movement.

Our algorithm also performs well in V1_03_difficult, which is the most challenging dataset with aggressive motion and great illumination change. The good initial guess from proposed method can compensate the negative influence from unstable feature tracking. The error plot compared with stereo OKVIS is shown in 9. Our system approximately achieves the same accuracy with this stereo algorithm.

B. Real World Experiment

We also test our algorithm onboard an aerial robot, as shown in Fig. 1(b). One forward-looking global shutter camera (MatrixVision mvBlueFOX-MLC200w) with 752×480 resolution. It is equipped with a 190-degree fisheye lens. A DJI A3 flight controller[2] is used both as the inertial measurement unit (IMU, ADXL278 and ADXRS290, 100Hz) and attitude stabilization control. The onboard computation resource includes an Intel i7-5500U CPU running at 3.00 GHz. A video of this experiment can be found in the supplementary material.

[2]http://www.dji.com/a3

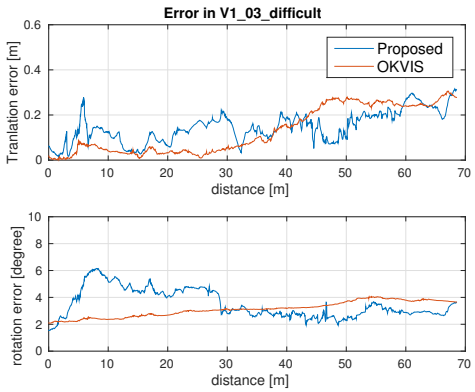

Fig. 9. Translation error and rotation error in V1_03_difficult.

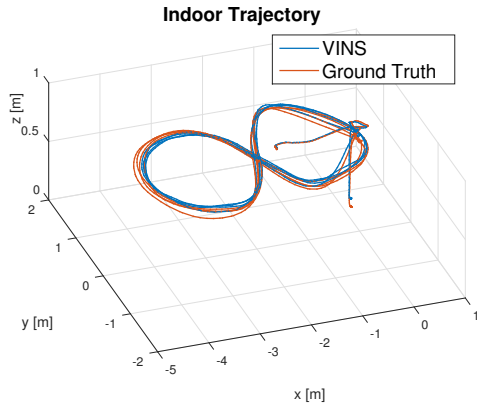

Fig. 10. The trajectory of the indoor onboard closed-loop experiment. After the visual-inertial system initialization on the fly, we manually control the quadrotor to the boundary and switch to the autonomous flight mode. The quadrotor flies following the designed trajectory. The designed trajectory is the figure of eight.

1) Indoor Closed-Loop Control: We perform real-time closed-loop control in this indoor experiment. The visual-inertial odometry serves as position, attitude, and velocity feedback in the control loop. To test the dynamic initialization capability, we start the visual-inertial system when the aerial robot is flying in the air, instead of launching the system on the ground stably. After launching the visual-inertial system, we add the VINS odometry into the control loop. Finally, we switch the aerial robot into autonomous flight mode, which will follow a designed trajectory.

The trajectory is shown in Fig. 10. The position along with time is shown in Fig. 11. At first, we manually control the quadrotor flying. At 7.5s, we launch the visual-inertial system when the quadrotor is flying in the air. The estimator outputs the odometry after initialization within one second. At 19.0s, we add the visual-inertial estimator into control loop, which helps stabilize the quadrotor in the air. We manually control the quadrotor to the start point. Finally, we switch the aerial robot into autonomous flight mode at 31.0s. The drone autonomously flies, following the trajectory

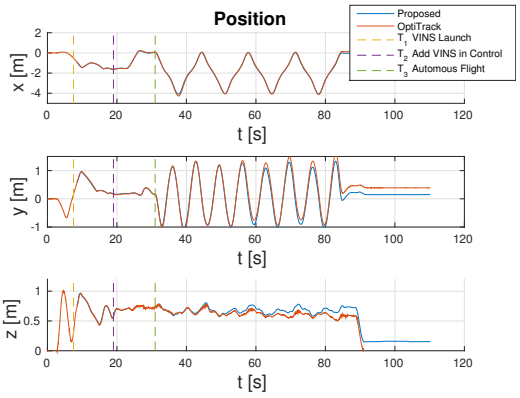

Fig. 11. Position of proposed system compared with OptiTrack in the indoor experiment. Three dash lines mean the time stamp of launching the visual-inertial system, adding odometry into control loop, and switching to autonomous flight.

under the visual-inertial feedback.

We compare our results with the ground truth which is provided by the OptiTrack system[3]. The blue line is the result from proposed estimator. The red line is the ground truth. Three dash lines represent three timestamps, when the proposed estimator is launched, the estimator is added into control loop, and the quadrotor starts autonomous flight respectively. The whole length in this indoor experiment is 58.12m. The final drift is [-0.13, -0.24, -0.16]m along x, y, and z respectively, which is 0.55% in percentage.

2) Outdoor Environments: Large scale environment is challenging for the monocular visual-inertial system. For visual measurement, a long movement which guarantees sufficient parallax between frames is required, which means a long time interval exists between spatial frames. However, the long time interval integration will seriously destroy the accuracy of IMU measurements. What's worse, when the drone flies smoothly in the high attitude, IMU measurements will degenerate and output nearly zero readings besides the gravity which will cause insufficient excitation to fully recover the scale.

To avoid long period integration, we maintain all frames instead of only spatial frames in the initialization procedure. Also, we reject degenerated movement and launch the proposed procedure only with sufficient excitation in inertial measurements. These adaptions make our algorithm perform well in large scale environments.

We verify our algorithm in the $100m$ by $80m$ outdoor area with altitude ranging from $40m$ to $90m$. We initialize the visual-inertial system when the drone is flying at 40 meters high, as shown in Fig. 12. The trajectory is compared with GPS. The total length is 575m, and the final drift is [-3.03, 0.18, 2.07]m along x, y, and z respectively, which is 0.64% in percentage.

[3]http://www.optitrack.com/

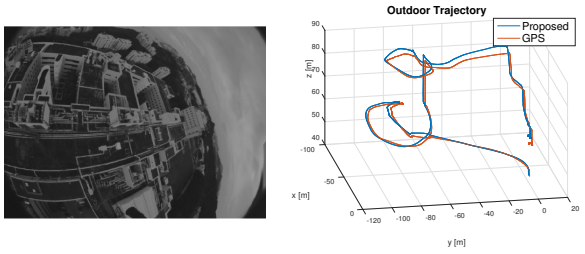

(a) (b)

Fig. 12. Outdoor experiment. (a)The view of the drone flying at high altitude with 45^o tiled-front looking fisheye camera. (b)The trajectory of our proposed method compared with GPS.

VI. Conclusion

In this paper, we propose a novel algorithm for the initialization of monocular visual-inertial estimators. Our initialization procedure provides initial guess (velocity, gravity vector, gyroscope bias, and depth of features) for nonlinear VINS estimator. These initial guesses are helpful to improve the performance of VINS by making it capable for on-the-fly initialization. We use real-world data in indoor closed-loop control and challenging outdoor environments to validate the practicability our proposed approach.

Finally, we are interested in fully autonomous navigation based on monocular visual-inertial system (VINS). Our first result, which is a drone navigation application with monocular dense mapping, obstacle avoidance, and path planning, was presented in [33]. We will do extensive research to further improve the accuracy and robustness of the system.

References

[1] G. Klein and D. Murray, "Parallel tracking and mapping for small ar workspaces," in *Mixed and Augmented Reality, 2007. ISMAR 2007. 6th IEEE and ACM International Symposium on*. IEEE, 2007, pp. 225–234.

[2] C. Forster, M. Pizzoli, and D. Scaramuzza, "SVO: Fast semi-direct monocular visual odometry," in *Proc. of the IEEE Int. Conf. on Robot. and Autom.*, Hong Kong, China, May 2014.

[3] J. Engel, T. Schöps, and D. Cremers, "Lsd-slam: Large-scale direct monocular slam," in *European Conference on Computer Vision*. Springer International Publishing, 2014, pp. 834–849.

[4] R. Mur-Artal, J. Montiel, and J. D. Tardos, "Orb-slam: a versatile and accurate monocular slam system," *IEEE Transactions on Robotics*, vol. 31, no. 5, pp. 1147–1163, 2015.

[5] J. Engel, V. Koltun, and D. Cremers, "Direct sparse odometry," *IEEE Transactions on Pattern Analysis and Machine Intelligence*, 2017.

[6] S. Leutenegger, S. Lynen, M. Bosse, R. Siegwart, and P. Furgale, "Keyframe-based visual-inertial odometry using nonlinear optimization," *Int. J. Robot. Research*, vol. 34, no. 3, pp. 314–334, Mar. 2014.

[7] S. Shen, Y. Mulgaonkar, N. Michael, and V. Kumar, "Initialization-free monocular visual-inertial estimation with application to autonomous MAVs," in *Proc. of the Int. Sym. on Exp. Robot.*, Marrakech, Morocco, Jun. 2014.

[8] S. Shen, N. Michael, and V. Kumar, "Tightly-coupled monocular visual-inertial fusion for autonomous flight of rotorcraft MAVs," in *Proc. of the IEEE Int. Conf. on Robot. and Autom.*, Seattle, WA, May 2015.

[9] M. Faessler, F. Fontana, C. Forster, and D. Scaramuzza, "Automatic re-initialization and failure recovery for aggressive flight with a monocular vision-based quadrotor," in *Proc. of the IEEE Int. Conf. on Robot. and Autom.* IEEE, 2015, pp. 1722–1729.

[10] M. Bloesch, S. Omari, M. Hutter, and R. Siegwart, "Robust visual inertial odometry using a direct ekf-based approach," in *Proc. of the IEEE/RSJ Int. Conf. on Intell. Robots and Syst.* IEEE, 2015, pp. 298–304.

[11] V. Usenko, J. Engel, J. Stückler, and D. Cremers, "Direct visual-inertial odometry with stereo cameras," in *Proc. of the IEEE Int. Conf. on Robot. and Autom.* IEEE, 2016, pp. 1885–1892.

[12] Z. Yang and S. Shen, "Monocular visual–inertial state estimation with online initialization and camera–imu extrinsic calibration," *IEEE Transactions on Automation Science and Engineering*, vol. 14, no. 1, pp. 39–51, 2017.

[13] A. I. Mourikis and S. I. Roumeliotis, "A multi-state constraint Kalman filter for vision-aided inertial navigation," in *Proc. of the IEEE Int. Conf. on Robot. and Autom.*, Roma, Italy, Apr. 2007, pp. 3565–3572.

[14] G. Sibley, L. Matthies, and G. Sukhatme, "Sliding window filter with application to planetary landing," *J. Field Robot.*, vol. 27, no. 5, pp. 587–608, Sep. 2010.

[15] J. A. Hesch, D. G. Kottas, S. L. Bowman, and S. I. Roumeliotis, "Consistency analysis and improvement of vision-aided inertial navigation," *IEEE Trans. Robot.*, vol. 30, no. 1, pp. 158–176, Feb. 2014.

[16] J. Kelly and G. S. Sukhatme, "Visual-inertial sensor fusion: Localization, mapping and sensor-to-sensor self-calibration," *Int. J. Robot. Research*, vol. 30, no. 1, pp. 56–79, Jan. 2011.

[17] S. Lynen, M. W. Achtelik, S. Weiss, M. Chli, and R. Siegwart, "A robust and modular multi-sensor fusion approach applied to mav navigation," in *Proc. of the IEEE/RSJ Int. Conf. on Intell. Robots and Syst.* IEEE, 2013, pp. 3923–3929.

[18] M. Li and A. Mourikis, "High-precision, consistent EKF-based visual-inertial odometry," *Int. J. Robot. Research*, vol. 32, no. 6, pp. 690–711, May 2013.

[19] A. Martinelli, "Closed-form solution of visual-inertial structure from motion," *Int. J. Comput. Vis.*, vol. 106, no. 2, pp. 138–152, 2014.

[20] J. Kaiser, A. Martinelli, F. Fontana, and D. Scaramuzza, "Simultaneous state initialization and gyroscope bias calibration in visual inertial aided navigation," *IEEE Robotics and Automation Letters*, vol. 2, no. 1, pp. 18–25, 2017.

[21] S. Weiss, R. Brockers, S. Albrektsen, and L. Matthies, "Inertial optical flow for throw-and-go micro air vehicles," in *Proc. of the IEEE Int. Conf. on Applications of Comput. Vis.* IEEE, 2015, pp. 262–269.

[22] A. Heyden and M. Pollefeys, "Multiple view geometry," *Emerging Topics in Computer Vision*, 2005.

[23] L. Kneip, S. Weiss, and R. Siegwart, "Deterministic initialization of metric state estimation filters for loosely-coupled monocular vision-inertial systems," in *Proc. of the IEEE/RSJ Int. Conf. on Intell. Robots and Syst.*, Sep. 2011, pp. 2235–2241.

[24] R. Mur-Artal and J. D. Tardos, "Visual-inertial monocular SLAM with map reuse," *arXiv preprint arXiv:1610.05949*, 2016.

[25] T. Lupton and S. Sukkarieh, "Visual-inertial-aided navigation for high-dynamic motion in built environments without initial conditions," *IEEE Trans. Robot.*, vol. 28, no. 1, pp. 61–76, Feb. 2012.

[26] C. Forster, L. Carlone, F. Dellaert, and D. Scaramuzza, "IMU preintegration on manifold for efficient visual-inertial maximum-a-posteriori estimation," in *Proc. of Robot.: Sci. and Syst.*, Rome, Italy, Jul. 2015.

[27] D. Nistér, "An efficient solution to the five-point relative pose problem," *IEEE transactions on pattern analysis and machine intelligence*, vol. 26, no. 6, pp. 756–770, 2004.

[28] B. Triggs, P. F. McLauchlan, R. I. Hartley, and A. W. Fitzgibbon, "Bundle adjustmenta modern synthesis," in *International workshop on vision algorithms*. Springer, 1999, pp. 298–372.

[29] J. Shi and C. Tomasi, "Good features to track," in *Proc. of the IEEE Int. Conf. on Pattern Recognition*, Seattle, WA, Jun. 1994, pp. 593–600.

[30] J. K. Suhr, "Kanade-lucas-tomasi (klt) feature tracker," *Computer Vision (EEE6503)*, pp. 9–18, 2009.

[31] Z. Yang and S. Shen, "Tightly-coupled visual-inertial sensor fusion based on IMU pre-integration," Hong Kong University of Science and Technology, Tech. Rep., 2016, URL: http://www.ece.ust.hk/~eeshaojie/vins2016zhenfei.pdf.

[32] P. Huber, "Robust estimation of a location parameter," *Annals of Mathematical Statistics*, vol. 35, no. 2, pp. 73–101, 1964.

[33] Y. Lin, F. Gao, T. Qin, W. Gao, T. Liu, W. Wu, Z. Yang, and S. Shen, "Autonomous aerial navigation using monocular visual-inertial fusion," *J. Field Robot.*, vol. 00, pp. 1–29, 2017.

[34] M. Burri, J. Nikolic, P. Gohl, T. Schneider, J. Rehder, S. Omari, M. W. Achtelik, and R. Siegwart, "The euroc micro aerial vehicle datasets," *The International Journal of Robotics Research*, 2016.